Decoupling Global and Local Representations from/for Image Generation

Xuezhe Ma[1], **Xiang Kong**[1], **Shanghang Zhang**[2], **Eduard Hovy**[1]
[1]Carnegie Mellon University
[2]University of California, Berkeley
{xuezhem,xiangk}@cs.cmu.edu, shzhang.pku@gmail.com, hovy@cmu.edu

Abstract

In this work, we propose a new generative model that is capable of automatically decoupling global and local representations of images in an entirely unsupervised setting. The proposed model utilizes the variational auto-encoding framework to learn a (low-dimensional) vector of latent variables to capture the global information of an image, which is fed as a conditional input to a flow-based invertible decoder with architecture borrowed from style transfer literature. Experimental results on standard image benchmarks demonstrate the effectiveness of our model in terms of density estimation, image generation and unsupervised representation learning. Importantly, this work demonstrates that with only architectural inductive biases, a generative model with a plain log-likelihood objective is capable of learning decoupled representations, requiring no explicit supervision. The code for our model is available at https://github.com/XuezheMax/wolf.

1 Introduction

Unsupervised learning of probabilistic models and meaningful representation learning are two central yet challenging problems in machine learning. Formally, let $X \in \mathcal{X}$ be the random variables of the observed data, e.g., X is an image. One goal of generative models is to learn the parameter θ such that the model distribution $P_\theta(X)$ can best approximate the true distribution $P(X)$. Throughout the paper, uppercase letters represent random variables and lowercase letters their realizations.

Unsupervised (disentangled) representation learning, besides data distribution estimation and data generation, is also a principal component in generative models. The goal is to identify and disentangle the underlying causal factors, to tease apart the underlying dependencies of the data, so that it becomes easier to understand, to classify, or to perform other tasks (Bengio et al., 2013). Unsupervised representation learning has spawned significant interests and a number of techniques (Chen et al., 2017a; Devlin et al., 2019; Hjelm et al., 2019) has emerged over the years to address this challenge. Among these generative models, VAE (Kingma and Welling, 2014; Rezende et al., 2014) and Generative (Normalizing) Flows (Dinh et al., 2014) have stood out for their simplicity and effectiveness.

1.1 Variational Auto-Encoders (VAEs)

VAE, as a member of latent variable models (LVMs), gains popularity for its capability of automatically learning meaningful (low-dimensional) representations from raw data. In the framework of VAEs, a set of latent variables $Z \in \mathcal{Z}$ are introduced, and the model distribution $P_\theta(X)$ is defined as the marginal of the joint distribution between X and Z:

$$p_\theta(x) = \int_{\mathcal{Z}} p_\theta(x, z) d\mu(z) = \int_{\mathcal{Z}} p_\theta(x|z) p_\theta(z) d\mu(z), \quad \forall x \in \mathcal{X}, \tag{1}$$

where the joint distribution $p_\theta(x, z)$ is factorized as the product of a prior $p_\theta(z)$ over the latent Z, and the "generative" distribution $p_\theta(x|z)$. $\mu(z)$ is the base measure on the latent space $\mathcal{Z}$.

Preprint. Under review.

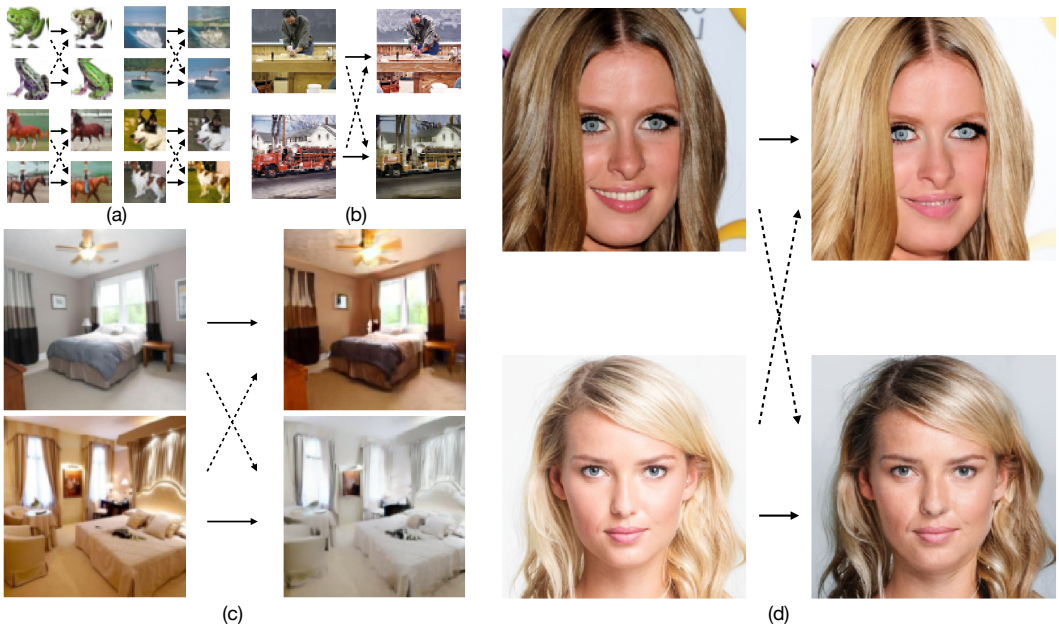

Figure 1: Examples of the switch operation, which switches the global representations of two images from four datasets: (a) CIFAR-10, (b) ImageNet, (c) LSUN Bedroom and (d) CelebA-HQ.

In general, this marginal likelihood is intractable to compute or differentiate directly, and Variational Inference (Wainwright et al., 2008) provides a solution to optimize the *evidence lower bound* (ELBO) an alternative objective by introducing a parametric *inference model* $q_\phi(z|x)$:

$$\mathrm{E}_{p(X)}\left[\log p_\theta(X)\right] \geq \mathrm{E}_{p(X)}\left[\mathrm{E}_{q_\phi(Z|X)}[\log p_\theta(X|Z)] - \mathrm{KL}(q_\phi(Z|X)||p_\theta(Z))\right] \tag{2}$$

where ELBO could be seen as an autoencoding loss with $q_\phi(z|x)$ being the encoder and $p_\theta(x|z)$ being the decoder, with the first term in the RHS in (2) as the reconstruction error.

1.2 Generative Flows

Put simply, generative flows (a.k.a normalizing flows) work by transforming a simple distribution (e.g. a simple Gaussian) into a complex on (e.g. the complex distribution of data $P(X)$) through a chain of invertible transformations.

Formally, a generative flow defines a bijection function $f : \mathcal{X} \to \Upsilon$ (with $g = f^{-1}$), where $\upsilon \in \Upsilon$ is a set of latent variables with simple prior distribution $p_\Upsilon(\upsilon)$. It provides us with a invertible transformation between X and Υ, whereby the generative process over X is defined straightforwardly:

$$\upsilon \sim p_\Upsilon(\upsilon), \quad \text{then } x = g_\theta(\upsilon). \tag{3}$$

An important insight behind generative flows is that given this bijection function, the change of the variable formula defines the model distribution on X by:

$$p_\theta(x) = p_\Upsilon\left(f_\theta(x)\right)\left|\det\left(\frac{\partial f_\theta(x)}{\partial x}\right)\right|, \tag{4}$$

where $\frac{\partial f_\theta(x)}{\partial x}$ is the Jacobian of f_θ at x. A stacked sequence of such invertible transformations is called a generative (normalizing) flow (Rezende and Mohamed, 2015):

$$X \underset{g_1}{\overset{f_1}{\longleftrightarrow}} H_1 \underset{g_2}{\overset{f_2}{\longleftrightarrow}} H2 \underset{g_3}{\overset{f_3}{\longleftrightarrow}} \cdots \underset{g_K}{\overset{f_K}{\longleftrightarrow}} \Upsilon,$$

where $f = f_1 \circ f_2 \circ \cdots \circ f_K$ is a flow of K transformations (omitting θ for brevity).

1.3 Problems of VAEs and Generative Flows

Despite their impressive successes, VAEs and generative flows still suffer their own problems.

Posterior Collapse in VAEs As discussed in Bowman et al. (2015), without further assumptions, the ELBO objective in (2) may not guide the model towards the intended role for the latent variables Z, or even learn uninformative Z with the observation that the KL term $\mathrm{KL}(q_\phi(Z|X)||p_\theta(Z))$ varnishes to zero. The essential reason of this *posterior collapse* problem is that, under absolutely unsupervised setting, the marginal likelihood-based objective incorporates no (direct) supervision on the latent space to characterize the latent variable Z with preferred properties w.r.t. representation learning.

Local Dependency in Generative Flows Generative flows suffer from the limitation of expressiveness and local dependency. Most generative flows tend to capture the dependency among features only locally, and are incapable of realistic synthesis of large images compared to GANs (Goodfellow et al., 2014). Unlike latent variable models, e.g. VAEs, which represent the high-dimensional data as coordinates in a latent low-dimensional space, the long-term dependencies that usually describe the global features of the data can only be propagated through a composition of transformations. Previous studies attempted to enlarge the receptive field by using a special design of parameterization like masked convolutions (Ma et al., 2019a) or attention mechanism (Ho et al., 2019).

In this paper, we propose a simple and effective generative model to simultaneously tackle the aforementioned challenges of VAEs and generative flows by leveraging their properties to complement each other. By embedding a generative flow in the VAE framework to model the decoder, the proposed model is able to learn decoupled representations which capture global and local information of images respectively in an entirely unsupervised manner. The key insight is to utilize the inductive biases from the model architecture design — leveraging the VAE framework equipped with a compression encoder to extract the global information in a low-dimensional representation, and a flow-based decoder which favors local dependencies to store the residual information into a local high-dimensional representation (§2). Experimentally, on four benchmark datasets for images, we demonstrate the effectiveness of our model on two aspects: (i) density estimation and image generation, by consistently achieving significant improvements over Glow (Kingma and Dhariwal, 2018), (ii) decoupled representation learning, by performing classification on learned representations the *switch operation* (see examples in Figure 1). Perhaps most strikingly, we demonstrate the feasibility of decoupled representation learning via plain likelihood-based generation, using only architectural inductive biases (§3).

2 Proposed Generative Model for Decoupled Representation Learning

We first illustrate the high-level insights of the architecture design of our generative model (shown in Figure 2) before detailing each component in the following sections.

In the training process of our generative model, we first feed the input image x into the encoder $q_\phi(z|x)$ in the VAE framework to compute the latent variable z. The encoder is designed to be a compression network, which compresses the high-dimensional image into a low-dimensional vector (§2.1). Through this compression process, the local information of an image x is enforced to be discarded, yielding representation z that captures the global information. Then we feed z as a conditional input to an flow-based decoder, which transforms x into the representation v with the same dimension (§2.2). Since the decoder is invertible, with z and v, we can exactly reconstruct the original image x. It indicates that z and v maintain all the information of x, and the reconstruction process can be regarded as an additional operation — adding z and v to recover x. In this way, we expect that the local information discarded in the compression process will be restored in v.

2.1 Compression Encoder

Following previous work, the variational posterior distribution $q_\phi(z|x)$, a.k.a encoder, models the latent variable Z as a diagonal Gaussian with learned mean and variance:

$$q_\phi(z|x) = \mathcal{N}(z; \mu(x), \sigma^2(x)) \tag{5}$$

where $\mu(\cdot)$ and $\sigma(\cdot)$ are neural networks. In the context of 2D images where x is a tensor of shape $[h \times w \times c]$ with spatial dimensions (h, w) and channel dimension c, the compression encoder maps each image x to a d_z-dimensional vector. d_z is the dimension of the latent space.

In this work, the motivation of the encoder is to compress the high-dimensional data x to low-dimensional latent variable z, i.e. $h \times w \times c \gg d_z$, to enforce the latent representation z to capture

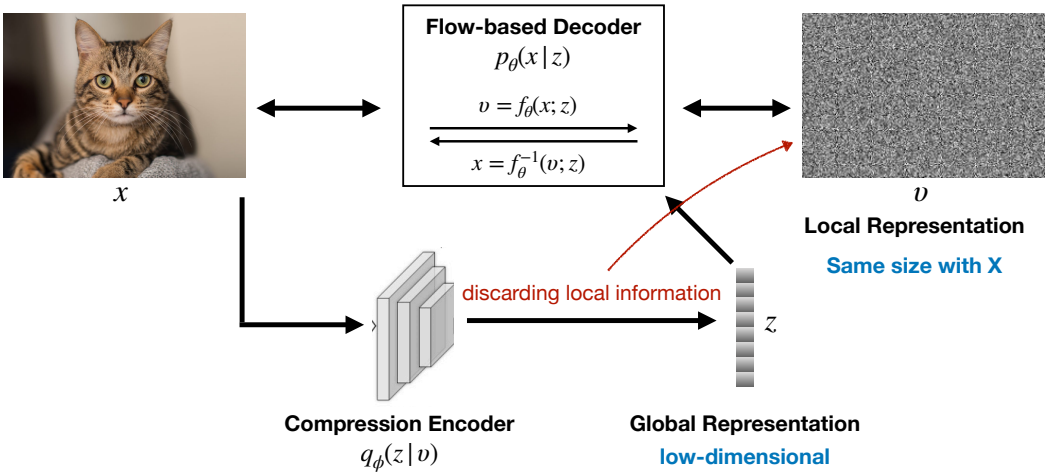

Figure 2: Diagram to illustrate the process of decoupling an image x into the global representation z and local representation v. The key insight is the architecture design of the compression encoder and the invertible decoder.

the global features of x. Furthermore, unlike previous studies on VAE based generative models for natural images (Kingma et al., 2016; Chen et al., 2017a; Ma et al., 2019b) that represented latent codes z as low-resolution feature maps[1], we represent z as an unstructured 1-dimensional vector to erase the local spatial dependencies. Concretely, we implement the encoder with a similar architecture in ResNet (He et al., 2016). The spatial downsampling is implemented by a 2-strided ResNet block with 3×3 filters. On top of these ResNet blocks, there is one more fully-connected layer with number of output units equal to $d_z \times 2$ to generate $\mu(x)$ and $\log \sigma^2(x)$ (details in Appendix B).

Zero initialization. Following Ma et al. (2019c), we initialize the weights of the last fully-connected layer that generates the μ and $\log \sigma^2$ values with zeros. This ensures that the posterior distribution is initialized as a simple normal distribution, which has been demonstrated helpful for training very deep neural networks more stably in the framework of VAEs.

2.2 Invertible Decoder based on Generative Flow

The flow-based decoder defines a (conditionally) invertible function $v = f_\theta(x; z)$, where v follows a standard normal distribution $v \sim \mathcal{N}(0, I)$. Conditioned on the latent variable z output from the encoder, we can reconstruct x with the inverse function $x = f_\theta^{-1}(v; z)$. The flow-based decoder adopts the main backbone architecture of Glow (Kingma and Dhariwal, 2018), where each step of flow consists of the same three types of elementary flows — actnorm, invertible 1×1 convolution and coupling (details in Appendix A).

Conditional Inputs in Affine Coupling Layers. To incorporate z as a conditional input to the decoder, we modify the neural networks for the scale and bias terms:

$$\begin{aligned} x_a, x_b &= \text{split}(x) \\ y_a &= x_a \\ y_b &= \text{s}(x_a, z) \odot x_b + \text{b}(x_a, z) \\ y &= \text{concat}(y_a, y_b), \end{aligned} \tag{6}$$

where $\text{s}()$ and $\text{b}()$ take both x_a and z as input. Specifically, each coupling layer includes three convolution layers where the first and last convolutions are 3×3, while the center convolution is 1×1. ELU (Clevert et al., 2015) is used as the activation function throughout the flow architecture:

$$x \rightarrow \text{Conv}_{3\times3} \rightarrow \text{ELU} \rightarrow \text{Conv}_{1\times1} \oplus \text{FC}(z) \rightarrow \text{ELU} \rightarrow \text{Conv}_{3\times3} \tag{7}$$

where $\text{FC}()$ refers to a linear full-connected layer and $\oplus$ is addition operation per channel between a 2D image and a 1D vector.

[1]For example, the latent codes of the images from CIFAR-10 corpus with size 32×32 are represented by 16 feature maps of size 8×8 in Kingma et al. (2016); Chen et al. (2017a).

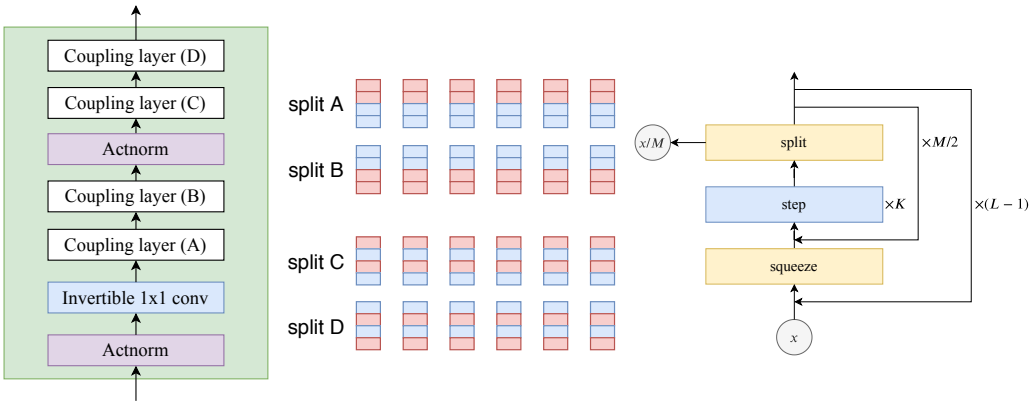

(a) One step of our flow (b) Four types of coupling layer splits (c) Fine-grained multi-scale architecture

Figure 3: The refined architecture of Glow that used in our decoder. (a) The architecture of one re-organized step. (b) The visualization of four split patterns for coupling layers, where the red color denotes x_a and the blue color denotes x_b. (c) The fine-grained version of multi-scale architecture.

Importantly, z is fed as conditional input to every coupling layers, unlike previous work (Agrawal and Dukkipati, 2016; Morrow and Chiu, 2019) where z is only used to learn the mean and variance of the underlying Gaussian of v. This design is inspired by the generator in Style-GAN (Karras et al., 2019), where the style-vector is added to each block of the generator. We conduct experiments to show the importance of this architectural design (see §3.1).

Refined Architecture of Glow. In this work, we refine the organization of these three elementary flows in one step (see Figure 3a) to reduce the total number of invertible 1×1 convolution flows. The season is that the cost and the numerical stability of computing or differentiating the determinant of the weight matrix becomes the practical bottleneck when the channel dimension c is considerably large for high-resolution images. To reduce the number of invertible 1×1 convolution flows while maintaining the permutation effect along the channel dimension, we use four split patterns for the $\mathrm{split}()$ function in (6) (see Figure 3b). The splits perform on the channel dimension with continuous and alternate patterns, respectively. For each pattern of split, we alternate x_a and x_b. Coupling layers with different split types alternate in one step of our flow, as illustrated in Figure 3a. We further replace the original multi-scale architecture with the fine-grained multi-scale architecture (Figure 3c) proposed in Ma et al. (2019a), with the same value of $M = 4$. Experimental improvements over Glow demonstrate the effectiveness of our refined architecture (§3.1).

2.3 Discussion

From the high-level view of the VAE encoder, the (indirect) supervision of learning global latent representation z comes from two sources of architectural inductive bias. First, the compression architecture, which takes a high-dimensional image as input and outputs a low-dimensional vector, encourages the encoder to discard local dependencies of the image. Second, the preference of the flow-based decoder for capturing local dependencies reinforces global information modeling of the encoder, since the all the information of the input image x needs to be preserved by z and v.

From the perspective of the flow-based decoder, the latent codes z provides the decoder with the imperative global information, which is essential to resolve the limitation of expressiveness due to local dependency. In this work, we utilize these complementary properties of the architectures of the encoder and decoder as inductive bias to attempt to decouple the global and local information of an image by storing them in separate representations.

3 Experiments

To evaluate our generative model, we conduct two groups of experiments on four benchmark datasets that are commonly used to evaluate deep generative models: CIFAR-10 (Krizhevsky and Hinton,

Table 1: Density estimation performance on four benchmark datasets. Results are reported in *bits/dim*.

Model	CIFAR-10 8-bit	ImageNet 8-bit	LSUN-bedroom 5-bit	LSUN-bedroom 8-bit	CelebA-HQ 5-bit	CelebA-HQ 8-bit
Autoregressive models						
IAF VAE (Kingma et al., 2016)	3.11	—	—	—	—	—
PixelRNN (Oord et al., 2016)	3.00	3.63	—	—	—	—
MAE (Ma et al., 2019b)	2.95	–	—	—	—	—
PixelCNN++ (Salimans et al., 2017)	2.92	–	—	—	—	—
PixelSNAIL (Chen et al., 2017b)	**2.85**	–				
SPN (Menick and Kalchbrenner, 2019)	—	**3.52**	—	—	**0.61**	—
Flow-based models						
Real NVP (Dinh et al., 2016)	3.49	3.98	—	—	—	—
Glow (Kingma and Dhariwal, 2018)	3.35	3.81	1.20	—	1.03	—
Glow: refined	3.33	3.77	1.19	1.98	1.02	1.99
Flow++ (Ho et al., 2019)	3.29	–	—	—	—	—
Residual Flow (Chen et al., 2019)	3.28	3.76	—	—	0.99	—
MaCow (Ma et al., 2019a)	3.28	3.75	1.16	—	**0.95**	—
Our model	**3.27**	**3.72**	**1.14**	**1.92**	0.97	**1.97**

2009), 64×64 downsampled version ImageNet (Oord et al., 2016), the *bedroom* category in LSUN (Yu et al., 2015) and the CelebA-HQ dataset (Karras et al., 2018)[2]. Unlike previous studies which performed experiments on 5-bit images from the LSUN and CelebA-HQ datasets, all the samples from the four datasets are 8-bit images in our experiments. All the models are trained by using affine coupling layers and uniform dequantization (Uria et al., 2013). Additional details on datasets, model architectures, and results of the conducted experiments are provided in Appendix C.

3.1 Generative Modeling

We begin our experiments with an evaluation on the performance of generative modeling, leaving the experiments of evaluating the quality of the decoupled global and local representations to §3.2. The baseline model we compare with is the refined Glow model, which is the exact architecture used in our flow-based decoder, except the conditional input z. Thus, the comparison with this baseline illustrates the effect of the decoupled representations on image generation. For the refined Glow model, we adjust the number of steps in each level so that there are similar numbers of coupling layers and parameters with the original Glow model for a fair comparison.

Density Estimation. Table 1 provides the negative log-likelihood scores in bits/dim (BPD) on the four benchmark datasets, along with the top-performing autoregressive models (first section) and flow-based generative models (second section). For a comprehensive comparison, we report results on 5-bit images from the LSUN and CelebA-HQ datasets with additive coupling layers. Our refined Glow model obtains better performance than the original one in Kingma and Dhariwal (2018), demonstrating the effectiveness of the refined architecture. The proposed generative model achieves state-of-the-art BPD on all the four standard benchmarks in the non-autoregressive category, except the 5-bit CelebA-HQ dataset.

Sample Quality For quantitative evaluation of sample quality, we report the Fréchet Inception Distance (FID) (Heusel et al., 2017) on CIFAR-10 in Table 2. Results marked with † and ‡ are taken from †Ostrovski et al. (2018) and ‡Heusel et al. (2017), respectively. Table 2 also provides scores of two energy-based models, EBM (Du and Mordatch, 2019) and NCSN (Song and Ermon, 2019). We see that our model obtains better FID scores than all the other explicit density models. In particular, the improvement over the refined Glow model on FID score demonstrates that learning decoupled representations is also helpful for realistic image synthesis.

Qualitatively, Figure 4 showcases some random samples for 8-bit CelebA-HQ 256×256 at temperature 0.7. More image samples, including samples on other datasets, are provided in Appendix F.

[2]For LSUN datasets, we use 128×128 downsampled version, and for CelebA-HQ we use 256×256 version.

Model	FID
PixelCNN†	65.93
PixelIQN†	49.46
DCGAN‡	37.11
WGAN-GP‡	29.30
EBM	40.58
NCSN	25.32
Glow	46.90
Glow: refined	46.50
Residual Flow	46.37
Our model	**37.52**

Table 2: FID scores on CIFAR-10.

Figure 4: 8-bit CelebA-HQ samples with temperature 0.7.

Effect of feeding z to every coupling layer. As mentioned in §2.2, we feed latent codes z to every coupling layer in the flow-based decoder. To investigate the importance of this design, we perform experiments on CIFAR-10 to compare our model with the baseline model where z is only used in the underlying Gaussian of v (Agrawal and Dukkipati, 2016; Morrow and Chiu, 2019). Table 3 gives the performance on BPD and FID score. Our model outperforms the baseline on both the two metrics, demonstrating the effectiveness of this design in our decoder.

Table 3: BPD and FID score.

Model	BPD	FID
Baseline	3.31	43.34
Ours	**3.27**	**37.52**

3.2 Decoupled Representation Learning

Image Classification As discussed above, good latent representation z need to capture global features that characterize the entire image, and disentangle the underlying causal factors. From this perspective, we follow the widely adopted *downstream linear evaluation protocol* (Oord et al., 2018; Hjelm et al., 2019) to train a linear classifier for image classification on the learned representations using all available training labels. The classification accuracy is a measure of the linear separability, which is commonly used as a proxy for disentanglement and mutual information between representations and class labels. We perform linear classification on CIFAR-10 using a support vector machine (SVM). Table 4 lists the classification accuracy of SVM on the representations of z and v, together with AAE (Makhzani et al., 2015), VAE (Kingma and Welling, 2014), BiGAN (Donahue et al., 2017) and Deep InfoMax (Hjelm et al., 2019). Results marked with † are token from Hjelm et al. (2019). Raw pixel is the baseline that directly training a classifier on the raw pixels of an image. The classification accuracy on the representation z is significantly better than that on v, indicating that z captures more global information, while v captures more local dependencies. Moreover, the accuracy of z outperforms Deep InfoMax, which is one of the state-of-the-art unsupervised representation learning methods via mutual information maximization.

Two-dimensional Interpolation Our generative model leads to the *two-dimensional interpolation*, where we linearly interpolate the two latent spaces z and v between two real images:

$$\begin{aligned} h(z) &= (1-\alpha)z_1 + \alpha z_2 \\ h(v) &= (1-\beta)v_1 + \beta v_2 \end{aligned} \tag{8}$$

where $\alpha, \beta \in [0, 1]$. z_1, v_1 and z_2, v_2 are the global and local representations of images x_1 and x_2, respectively. Figure 5 shows one interpolation example from CelebA-HQ, where the images on the left top and right bottom corners are the real images[3]. The switch operation is two special cases of the two-dimensional interpolation with $(\alpha = 1, \beta = 0)$ and $(\alpha = 0, \beta = 1)$. More examples of interpolation and switch operation are provided in Appendix D.

[3]For each column, α ranges in $[0.0, 0.25, 0.5, 0.75, 1.0]$; while for each raw, β ranges in $[0.0, 0.1, 0.2, 0.3, 0.4, 0.5, 0.6, 0.7, 0.8, 0.9, 1.0]$

Model	Acc.
Raw pixel	35.32
AAE†	37.76
VAE†	39.59
BiGAN†	44.90
Deep InfoMax‡	49.62
Our (z)	59.53
Our (v)	17.16

Table 4: Classification accuracy.

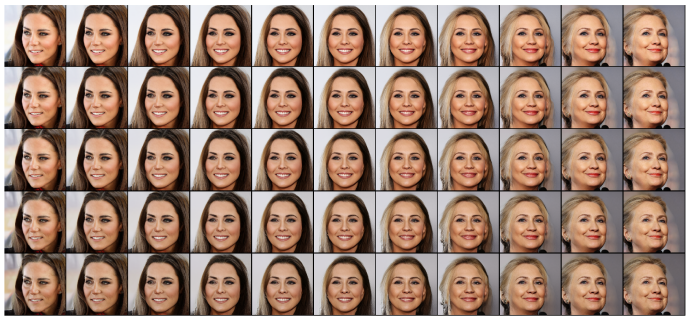

Figure 5: 2-dimensional linear interpolation between real images.

4 Related Work

Combination of VAEs and Generative Flows. In the literature of combining VAEs and generative flows, one direction of research is to use generative flows as an inference machine in variational inference for continuous latent variable models (Kingma et al., 2016; Van Den Berg et al., 2018). Another direction is to incorporate generative flows in the VAE framework as a trainable component, such as the prior (Chen et al., 2017a) or the decoder (Agrawal and Dukkipati, 2016; Morrow and Chiu, 2019). Recently, two contemporaneous work (Huang et al., 2020; Chen et al., 2020) explore the idea of constructing an invertible flow-based model on an augmented input space by augmenting the original data with an additional random variable. The main difference between these work and ours is the purpose of introducing the latent variables and using generative flows. In Huang et al. (2020); Chen et al. (2020), the latent variables are utilized to augment the input with extra dimensions to improve the expressivenss of the bijective mapping in generative flows. Our generative model, on the other hand, aims to learn representations with decoupled information, and the design of the latent variables and the flow-based decoder architecture is to accomplish this goal.

Disentangled Representation Learning. Disentanglement learning (Bengio et al., 2013; Mathieu et al., 2016) recently becomes a popular topic in representation learning. Creating representations where each dimension is independent and corresponds to a particular attribute have been explored in several approaches, including VAE variants (Higgins et al., 2017; Kim and Mnih, 2018; Chen et al., 2018), adversarial training (Mathieu et al., 2016; Karras et al., 2019) and mutual information maximization/regularization (Chen et al., 2016; Hjelm et al., 2019; Sanchez et al., 2019). Different from these work which attempted to learn factorial representations for disentanglement, we aim to learn two separate representations to decouple the global and local information.

Neural Style Transfer. From the visualization, the switch operation of our model is also (empirically) related to neural style transfer of natural images (Gatys et al., 2015; Johnson et al., 2016; Jing et al., 2019) — the global and local representations in our model appear to correspond to the *style* and *content* representations in neural style transfer models. The main difference is that the global and local representations in our model are learned in unsupervised manner, while the content and style representations in neural style transfer models are usually extracted from a pre-trained classification network (VGG network) (Simonyan and Zisserman, 2014). It is an interesting direction of future work to further investigate the relation between our learned decoupled representations and the content and style representations in neural style transfer models.

5 Conclusion

In this paper, we propose a simple and effective generative model that embeds a generative flow as decoder in the VAE framework. Simple as it appears to be, our model is capable of automatically decoupling global and local representations of images in an entirely unsupervised setting. Experimental results on standard image benchmarks demonstrate the effectiveness of our model on generative modeling and representation learning. Importantly, we demonstrate the feasibility of decoupled representation learning via plain likelihood-based generation, using only architectural inductive biases. Moreover, the two-dimensional interpolation supported by our model, with the switch operation as a special case, is an important step towards controllable image manipulation.

References

Siddharth Agrawal and Ambedkar Dukkipati. Deep variational inference without pixel-wise reconstruction. *arXiv preprint arXiv:1611.05209*, 2016.

Yoshua Bengio, Aaron Courville, and Pascal Vincent. Representation learning: A review and new perspectives. *IEEE transactions on pattern analysis and machine intelligence*, 35(8):1798–1828, 2013.

Samuel R Bowman, Luke Vilnis, Oriol Vinyals, Andrew M Dai, Rafal Jozefowicz, and Samy Bengio. Generating sentences from a continuous space. *arXiv preprint arXiv:1511.06349*, 2015.

Jianfei Chen, Cheng Lu, Biqi Chenli, Jun Zhu, and Tian Tian. Vflow: More expressive generative flows with variational data augmentation. *arXiv preprint arXiv:2002.09741*, 2020.

Tian Qi Chen, Xuechen Li, Roger B Grosse, and David K Duvenaud. Isolating sources of disentanglement in variational autoencoders. In *Advances in Neural Information Processing Systems*, pages 2610–2620, 2018.

Tian Qi Chen, Jens Behrmann, David K Duvenaud, and Jörn-Henrik Jacobsen. Residual flows for invertible generative modeling. In *Advances in Neural Information Processing Systems*, pages 9913–9923, 2019.

Xi Chen, Yan Duan, Rein Houthooft, John Schulman, Ilya Sutskever, and Pieter Abbeel. Infogan: Interpretable representation learning by information maximizing generative adversarial nets. In *Advances in neural information processing systems*, pages 2172–2180, 2016.

Xi Chen, Diederik P Kingma, Tim Salimans, Yan Duan, Prafulla Dhariwal, John Schulman, Ilya Sutskever, and Pieter Abbeel. Variational lossy autoencoder. In *Proceedings of the 5th International Conference on Learning Representations (ICLR-2017)*, Toulon, France, April 2017a.

Xi Chen, Nikhil Mishra, Mostafa Rohaninejad, and Pieter Abbeel. Pixelsnail: An improved autoregressive generative model. *arXiv preprint arXiv:1712.09763*, 2017b.

Djork-Arné Clevert, Thomas Unterthiner, and Sepp Hochreiter. Fast and accurate deep network learning by exponential linear units (elus). *arXiv preprint arXiv:1511.07289*, 2015.

Jacob Devlin, Ming-Wei Chang, Kenton Lee, and Kristina Toutanova. Bert: Pre-training of deep bidirectional transformers for language understanding. In *Proceedings of the 2019 Conference of the North American Chapter of the Association for Computational Linguistics: Human Language Technologies, Volume 1 (Long and Short Papers)*, pages 4171–4186, 2019.

Laurent Dinh, David Krueger, and Yoshua Bengio. Nice: Non-linear independent components estimation. *arXiv preprint arXiv:1410.8516*, 2014.

Laurent Dinh, Jascha Sohl-Dickstein, and Samy Bengio. Density estimation using real nvp. *arXiv preprint arXiv:1605.08803*, 2016.

Jeff Donahue, Philipp Krähenbühl, and Trevor Darrell. Adversarial feature learning. In *Proceedings of the 5th International Conference on Learning Representations (ICLR-2017)*, Toulon, France, April 2017.

Yilun Du and Igor Mordatch. Implicit generation and modeling with energy based models. In *Advances in Neural Information Processing Systems*, pages 3603–3613, 2019.

Leon A Gatys, Alexander S Ecker, and Matthias Bethge. A neural algorithm of artistic style. *arXiv preprint arXiv:1508.06576*, 2015.

Ian Goodfellow, Jean Pouget-Abadie, Mehdi Mirza, Bing Xu, David Warde-Farley, Sherjil Ozair, Aaron Courville, and Yoshua Bengio. Generative adversarial nets. In *Advances in neural information processing systems (NIPS-2014)*, pages 2672–2680, 2014.

Kaiming He, Xiangyu Zhang, Shaoqing Ren, and Jian Sun. Deep residual learning for image recognition. In *Proceedings of the IEEE conference on computer vision and pattern recognition*, pages 770–778, 2016.

Martin Heusel, Hubert Ramsauer, Thomas Unterthiner, Bernhard Nessler, and Sepp Hochreiter. Gans trained by a two time-scale update rule converge to a local nash equilibrium. In *Advances in neural information processing systems*, pages 6626–6637, 2017.

Irina Higgins, Loic Matthey, Arka Pal, Christopher Burgess, Xavier Glorot, Matthew Botvinick, Shakir Mohamed, and Alexander Lerchner. beta-vae: Learning basic visual concepts with a constrained variational framework. In *Proceedings of the 5th International Conference on Learning Representations (ICLR-2017)*, Toulon, France, April 2017.

R Devon Hjelm, Alex Fedorov, Samuel Lavoie-Marchildon, Karan Grewal, Phil Bachman, Adam Trischler, and Yoshua Bengio. Learning deep representations by mutual information estimation and maximization. In *International Conference on Learning Representations (ICLR)*, 2019.

Jonathan Ho, Xi Chen, Aravind Srinivas, Yan Duan, and Pieter Abbeel. Flow++: Improving flow-based generative models with variational dequantization and architecture design. In *International Conference on Machine Learning*, pages 2722–2730, 2019.

Chin-Wei Huang, Laurent Dinh, and Aaron Courville. Augmented normalizing flows: Bridging the gap between generative flows and latent variable models. *arXiv preprint arXiv:2002.07101*, 2020.

Sergey Ioffe and Christian Szegedy. Batch normalization: Accelerating deep network training by reducing internal covariate shift. In *International Conference on Machine Learning*, pages 448–456, 2015.

Yongcheng Jing, Yezhou Yang, Zunlei Feng, Jingwen Ye, Yizhou Yu, and Mingli Song. Neural style transfer: A review. *IEEE transactions on visualization and computer graphics*, 2019.

Justin Johnson, Alexandre Alahi, and Li Fei-Fei. Perceptual losses for real-time style transfer and super-resolution. In *European conference on computer vision*, pages 694–711. Springer, 2016.

Tero Karras, Timo Aila, Samuli Laine, and Jaakko Lehtinen. Progressive growing of gans for improved quality, stability, and variation. In *International Conference on Learning Representations (ICLR)*, 2018.

Tero Karras, Samuli Laine, and Timo Aila. A style-based generator architecture for generative adversarial networks. In *2019 IEEE/CVF Conference on Computer Vision and Pattern Recognition (CVPR)*, pages 4396–4405. IEEE, 2019.

Hyunjik Kim and Andriy Mnih. Disentangling by factorising. In *International Conference on Machine Learning*, pages 2649–2658, 2018.

Diederik P Kingma and Jimmy Ba. Adam: A method for stochastic optimization. *arXiv preprint arXiv:1412.6980*, 2014.

Diederik P Kingma and Max Welling. Auto-encoding variational bayes. In *Proceedings of the 2th International Conference on Learning Representations (ICLR-2014)*, Banff, Canada, April 2014.

Diederik P Kingma, Tim Salimans, Rafal Jozefowicz, Xi Chen, Ilya Sutskever, and Max Welling. Improved variational inference with inverse autoregressive flow. In *Advances in Neural Information Processing Systems*, pages 4743–4751, 2016.

Durk P Kingma and Prafulla Dhariwal. Glow: Generative flow with invertible 1x1 convolutions. In *Advances in Neural Information Processing Systems*, pages 10236–10245, 2018.

Alex Krizhevsky and Geoffrey Hinton. Learning multiple layers of features from tiny images. Technical report, Citeseer, 2009.

Xuezhe Ma, Xiang Kong, Shanghang Zhang, and Eduard Hovy. Macow: Masked convolutional generative flow. In *Advances in Neural Information Processing Systems 33*. Curran Associates, Inc., 2019a.

Xuezhe Ma, Chunting Zhou, and Eduard Hovy. MAE: Mutual posterior-divergence regularization for variational autoencoders. In *International Conference on Learning Representations (ICLR)*, 2019b.

Xuezhe Ma, Chunting Zhou, Xian Li, Graham Neubig, and Eduard Hovy. Flowseq: Non-autoregressive conditional sequence generation with generative flow. In *Proceedings of EMNLP-2019*, Hong Kong, November 2019c.

Alireza Makhzani, Jonathon Shlens, Navdeep Jaitly, Ian Goodfellow, and Brendan Frey. Adversarial autoencoders. *arXiv preprint arXiv:1511.05644*, 2015.

Michael F Mathieu, Junbo Jake Zhao, Junbo Zhao, Aditya Ramesh, Pablo Sprechmann, and Yann LeCun. Disentangling factors of variation in deep representation using adversarial training. In *Advances in neural information processing systems*, pages 5040–5048, 2016.

Jacob Menick and Nal Kalchbrenner. Generating high fidelity images with subscale pixel networks and multidimensional upscaling. In *International Conference on Learning Representations (ICLR)*, 2019.

Rogan Morrow and Wei-Chen Chiu. Variational autoencoders with normalizing flow decoders. *OpenReview*, 2019.

Aaron van den Oord, Nal Kalchbrenner, and Koray Kavukcuoglu. Pixel recurrent neural networks. In *Proceedings of International Conference on Machine Learning (ICML-2016)*, 2016.

Aaron van den Oord, Yazhe Li, and Oriol Vinyals. Representation learning with contrastive predictive coding. *arXiv preprint arXiv:1807.03748*, 2018.

Georg Ostrovski, Will Dabney, and Remi Munos. Autoregressive quantile networks for generative modeling. In *International Conference on Machine Learning*, pages 3936–3945, 2018.

Danilo Jimenez Rezende and Shakir Mohamed. Variational inference with normalizing flows. *arXiv preprint arXiv:1505.05770*, 2015.

Danilo Jimenez Rezende, Shakir Mohamed, and Daan Wierstra. Stochastic backpropagation and approximate inference in deep generative models. In *Proceedings of the 31st International Conference on Machine Learning (ICML-2014)*, pages 1278–1286, Bejing, China, 22–24 Jun 2014.

Tim Salimans, Andrej Karpathy, Xi Chen, Diederik P Kingma, and Yaroslav Bulatov. Pixelcnn++: A pixelcnn implementation with discretized logistic mixture likelihood and other modifications. In *International Conference on Learning Representations (ICLR)*, 2017.

Eduardo Hugo Sanchez, Mathieu Serrurier, and Mathias Ortner. Learning disentangled representations via mutual information estimation. *arXiv preprint arXiv:1912.03915*, 2019.

Karen Simonyan and Andrew Zisserman. Very deep convolutional networks for large-scale image recognition. *arXiv preprint arXiv:1409.1556*, 2014.

Yang Song and Stefano Ermon. Generative modeling by estimating gradients of the data distribution. In *Advances in Neural Information Processing Systems*, pages 11895–11907, 2019.

Benigno Uria, Iain Murray, and Hugo Larochelle. Rnade: The real-valued neural autoregressive density-estimator. In *Advances in Neural Information Processing Systems*, pages 2175–2183, 2013.

Rianne Van Den Berg, Leonard Hasenclever, Jakub M Tomczak, and Max Welling. Sylvester normalizing flows for variational inference. In *34th Conference on Uncertainty in Artificial Intelligence 2018, UAI 2018*, pages 393–402, 2018.

Martin J Wainwright, Michael I Jordan, et al. Graphical models, exponential families, and variational inference. *Foundations and Trends® in Machine Learning*, 1(1–2):1–305, 2008.

Fisher Yu, Yinda Zhang, Shuran Song, Ari Seff, and Jianxiong Xiao. Lsun: Construction of a large-scale image dataset using deep learning with humans in the loop. *arXiv preprint arXiv:1506.03365*, 2015.

Appendix: Decoupling Global and Local Representations from/for Image Generation

All the details of implementation and experiments are provided in our code https://github.com/XuezheMax/wolf.

A Glow

Flow-based generative models focus on certain types of transformations f_θ that allow (i) the inverse functions g_θ and Jacobian determinants to be tractable and efficient to compute and (ii) f_θ to be expressive. Most work within this line of research is dedicated to designing invertible transformations to enhance the expressiveness while maintaining the computational efficiency (Kingma and Dhariwal, 2018; Ma et al., 2019a; Ho et al., 2019; Chen et al., 2019), among which Glow (Kingma and Dhariwal, 2018) has stood out for its simplicity and effectiveness. The following briefly describes the three types of transformations that comprise Glow, which (in a refined version) is adopted as the backbone architecture of the flow-based decoder in our generative model (detailed in Appendix B).

Actnorm. Kingma and Dhariwal (2018) proposed an activation normalization layer (Actnorm) as an alternative for batch normalization (Ioffe and Szegedy, 2015) to alleviate the challenges in model training. Similar to batch normalization, Actnorm performs an affine transformation of the activations using a scale and bias parameter per channel for 2D images, such that

$$y_{i,j} = s \odot x_{i,j} + b, \tag{1}$$

where both x and y are tensors of shape $[h \times w \times c]$ with spatial dimensions (h, w) and channel dimension c.

Invertible 1×1 convolution. To incorporate a permutation along the channel dimension, Glow includes a trainable invertible 1×1 convolution layer to generalize the permutation operation as:

$$y_{i,j} = W x_{i,j}, \tag{2}$$

where W is the weight matrix with shape $c \times c$.

Affine Coupling Layers. Following Dinh et al. (2016), Glow includes affine coupling layers in its architecture of:

$$\begin{aligned} x_a, x_b &= \mathrm{split}(x) \\ y_a &= x_a \\ y_b &= \mathrm{s}(x_a) \odot x_b + \mathrm{b}(x_a) \\ y &= \mathrm{concat}(y_a, y_b), \end{aligned} \tag{3}$$

where $\mathrm{s}(x_a)$ and $\mathrm{b}(x_a)$ are outputs of two neural networks with x_a as input. The $\mathrm{split}()$ and $\mathrm{concat}()$ functions perform operations along the channel dimension.

B Implementation Details

B.1 Compression encoder

The encoder first compresses the input image of size $[h \times h \times c]$ to the low-resolution tensor of size $4 \times 4 \times c'$. Then, with a fully-connected layer, the encoder transforms the output tensor to a vector of dimension d_z. Concretely, to compress the high-resolution images to low-resolution tensors, the encoder consists of levels of ResNet blocks (He et al., 2016). At each level, there are two ResNet blocks with the same number of hidden units and strides 1 and 2, respectively. Thus, after each level the input is compressed to half of the spatial dimensions: from $h \times h$ to $\frac{h}{2} \times \frac{h}{2}$. ELU (Clevert et al., 2015) is used as the activation function throughout the encoder architecture.

B.2 Scale term in affine coupling layers

To model the scale term s in (6), a straight-forward way is to take the output of the neural network as the logarithm of s. Formally, let u denote as the output from the neural network described in (7).

Then we can compute s by taking the exponential function of u:

$$s = \exp(u)$$

In practice, however, we found this formulation leads to numerical issues in model training. In our implementation, we calculate s in the following way:

$$s = \alpha \cdot \tanh(\frac{u}{2}) + 1$$

where the constant $\alpha \in (0, 1)$. In this formulation, we restrict s in the range of $[1 - \alpha, 1 + \alpha]$. For ImageNet, we set $\alpha = 0.5$ while for other datasets we used $\alpha = 1.0$. In the experiments, we found this formulation not only improved the numerical stability but also achieved better performance on density estimation and FID scores.

B.3 Prior distribution in VAEs

In this work, the prior distribution $p_\theta(z)$ in VAE is modeled with a generative flow with architecture similar to Glow. The generative flow also consists of three elementary invertible transformations: actnorm, invertible linear layer and affine coupling layer. The actnorm and invertible linear layer is similar to those in Ma et al. (2019c), with the difference that we did not use the multi-head mechanism. The affine coupling layer is similar to the one in Glow, which applies the split function across the dimension d_z. The neural networks for the scale and bias terms in affine coupling layers are implemented with multi-layer perceptrons (MLP).

C Experimental Details

C.1 Preprocessing

We used random horizontal flipping for CIFAR10, and CelebA-HQ 256. For CIFAR-10, we also used random cropping after reflection padding with 4 pixels. For LSUN 128, we first centre cropped the original image, then downsampled to size 128×128.

C.2 Optimization

Parameter optimization is performed with the Adam optimizer (Kingma and Ba, 2014) with $\beta = (0.9, 0.999)$ and $\epsilon = 1\mathrm{e} - 8$. Warmup training is applied to all the experiments: the learning rate linearly increases to the initial learning rate $1\mathrm{e} - 3$. Then we use exponential decay to decrease the learning rate with decay rate is 0.999997.

C.3 Hyper-parameters

Table 5: Hyper-parameters in our experiments.

Dataset	batch size	latent dim d_z	weight decay	# updates of warmup
CIFAR-10, 32×32	512	64	$1e-6$	50
ImageNet, 64×64	256	128	$5e-4$	200
LSUN, 128×128	256	256	$5e-4$	200
CelebA-HQ, 256×256	40	256	$5e-4$	200

D Examples for two-dimensional interpolation

Figure 6: Interpolation operation between samples from 8-bit, 256×256 CelebA-HQ.

E More samples for switch operation

E.1 CelebA-HQ

Figure 7: Switch operation between samples from 8-bit, 256×256 CelebA-HQ.

E.2 CIFAR-10 & ImageNet

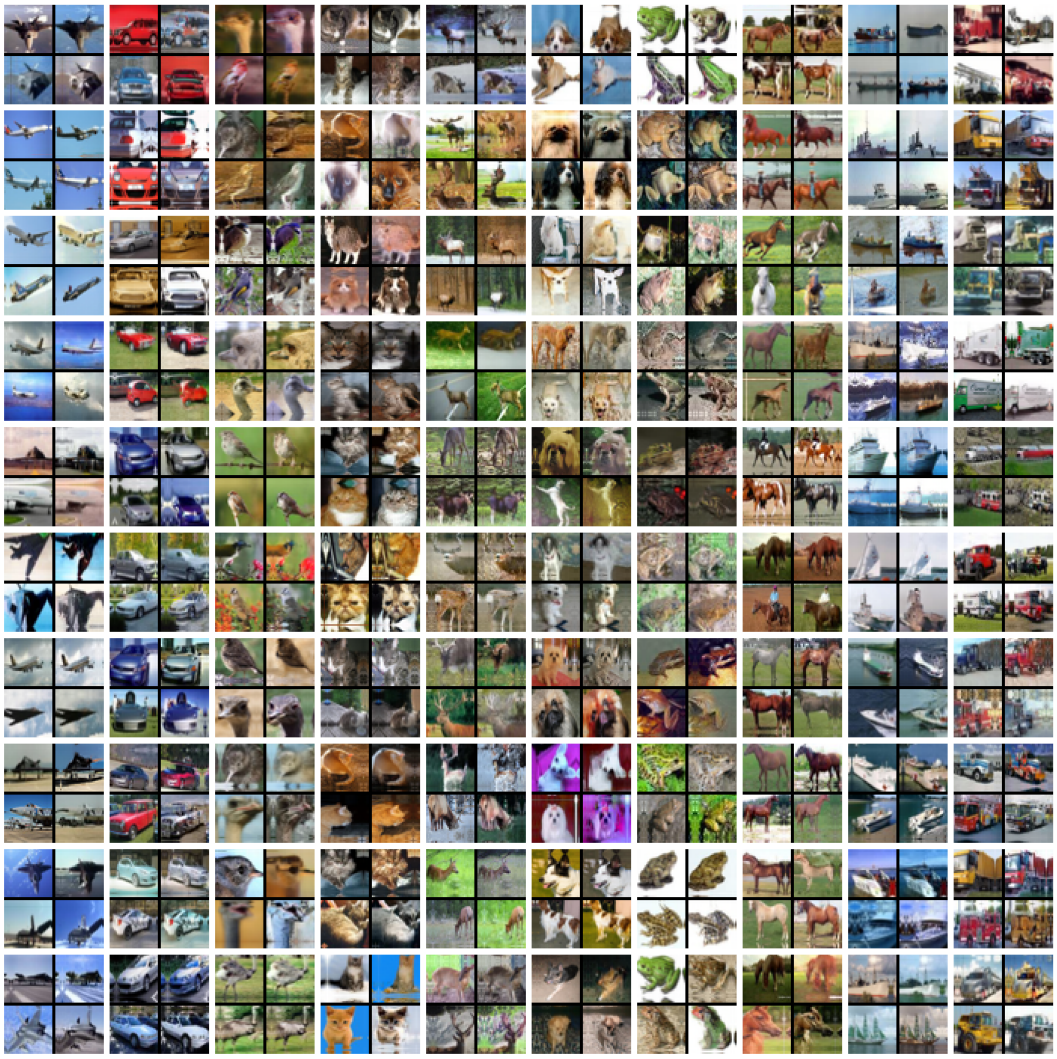

Figure 8: Switch operation between samples within the same class from 8-bit, 32×32 CIFAR-10.

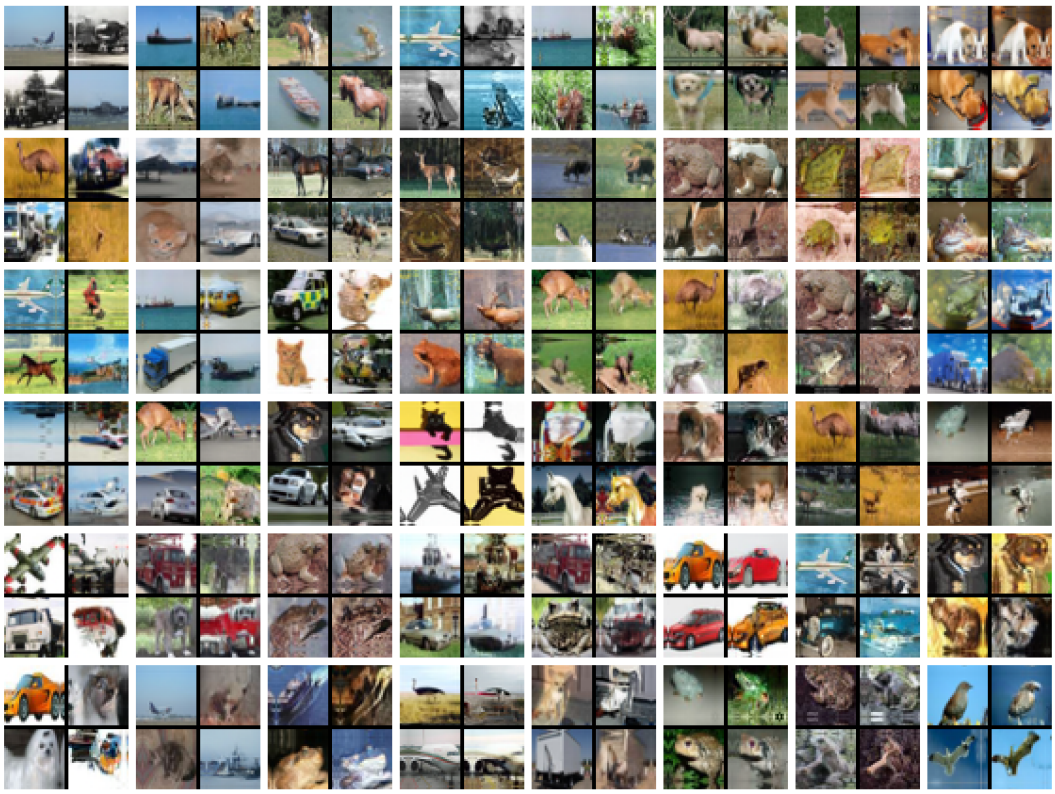

Figure 9: Switch operation between samples across different classes from 8-bit, 32×32 CIFAR-10.

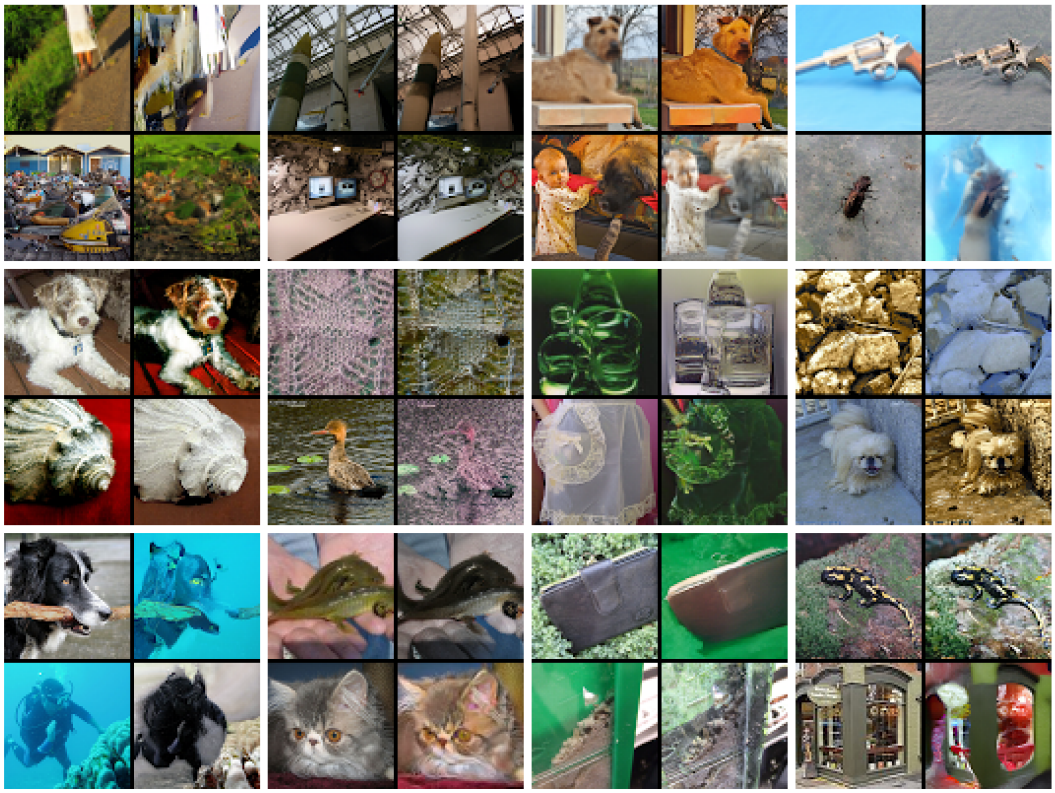

Figure 10: Switch operation between samples from 8-bit, 64×64 imagenet.

E.3 LSUN-Bedroom

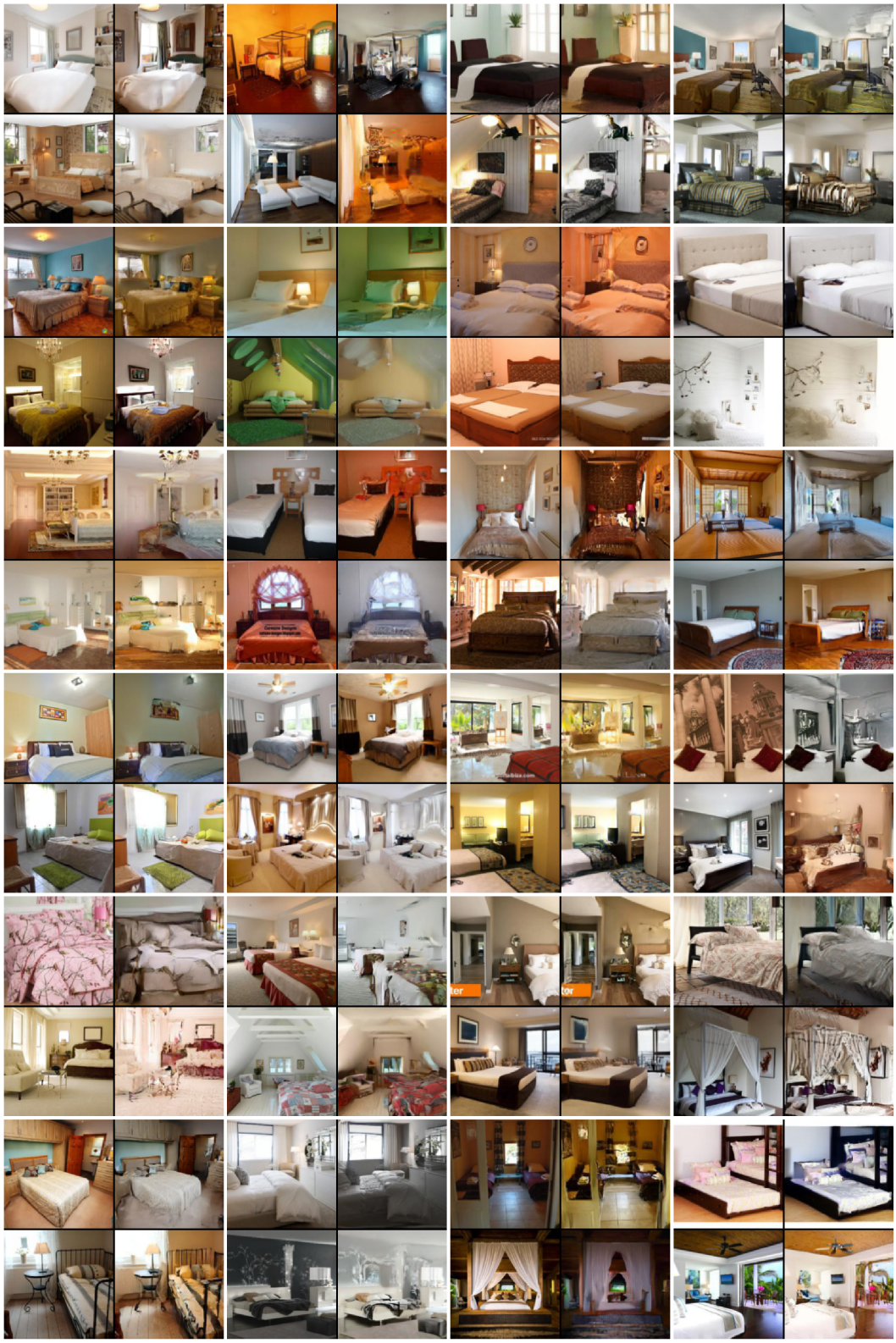

Figure 11: Switch operation between samples from 8-bit, 128×128 LSUN bedroom.

F More Image Samples

F.1 CelebA-HQ

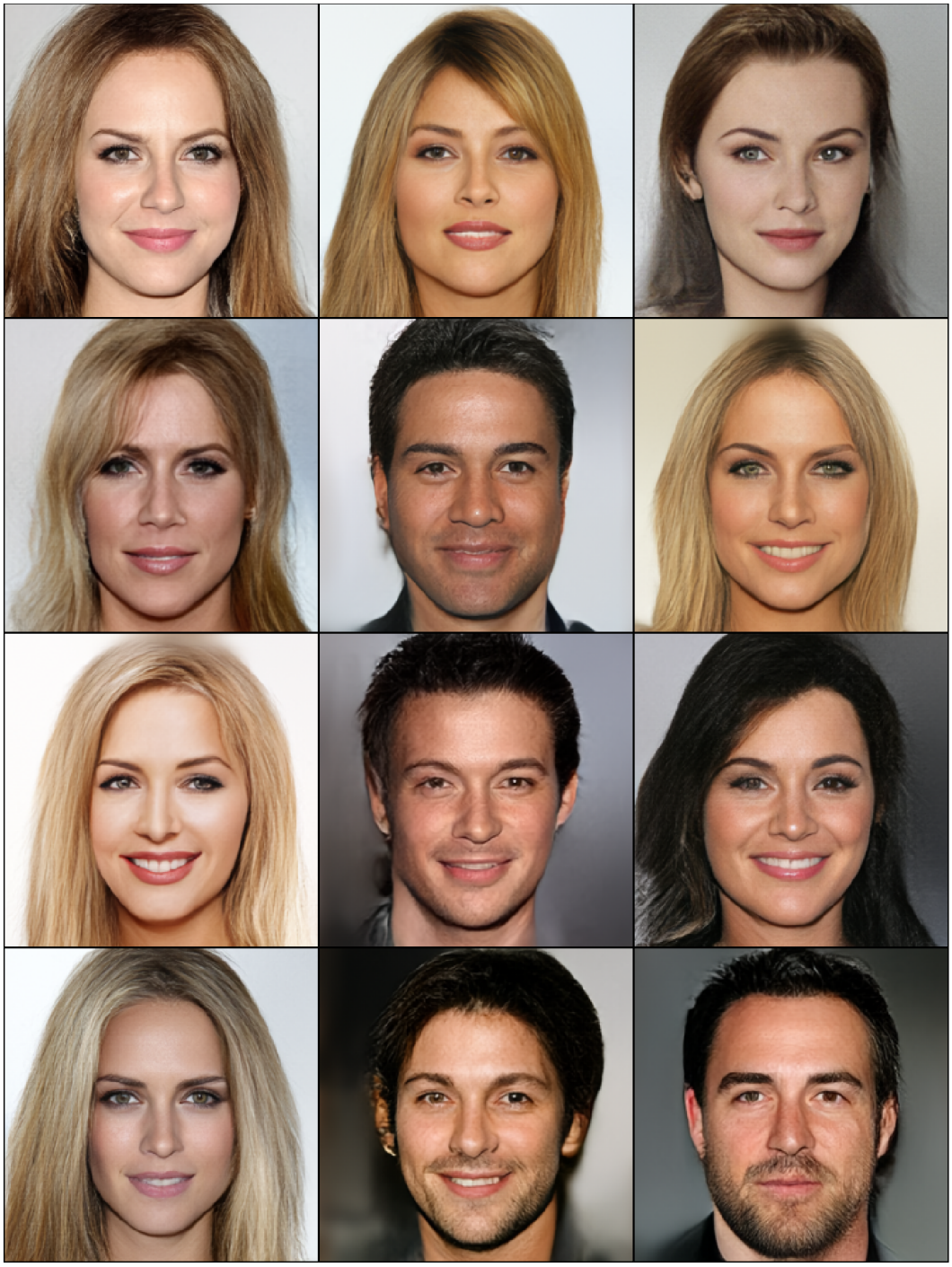

Figure 12: Samples from 8-bit, 256×256 CelebA-HQ with temperature 0.7.

Figure 13: Samples from 8-bit, 256×256 CelebA-HQ with temperature 1.0.

F.2 LSUN-Bedroom

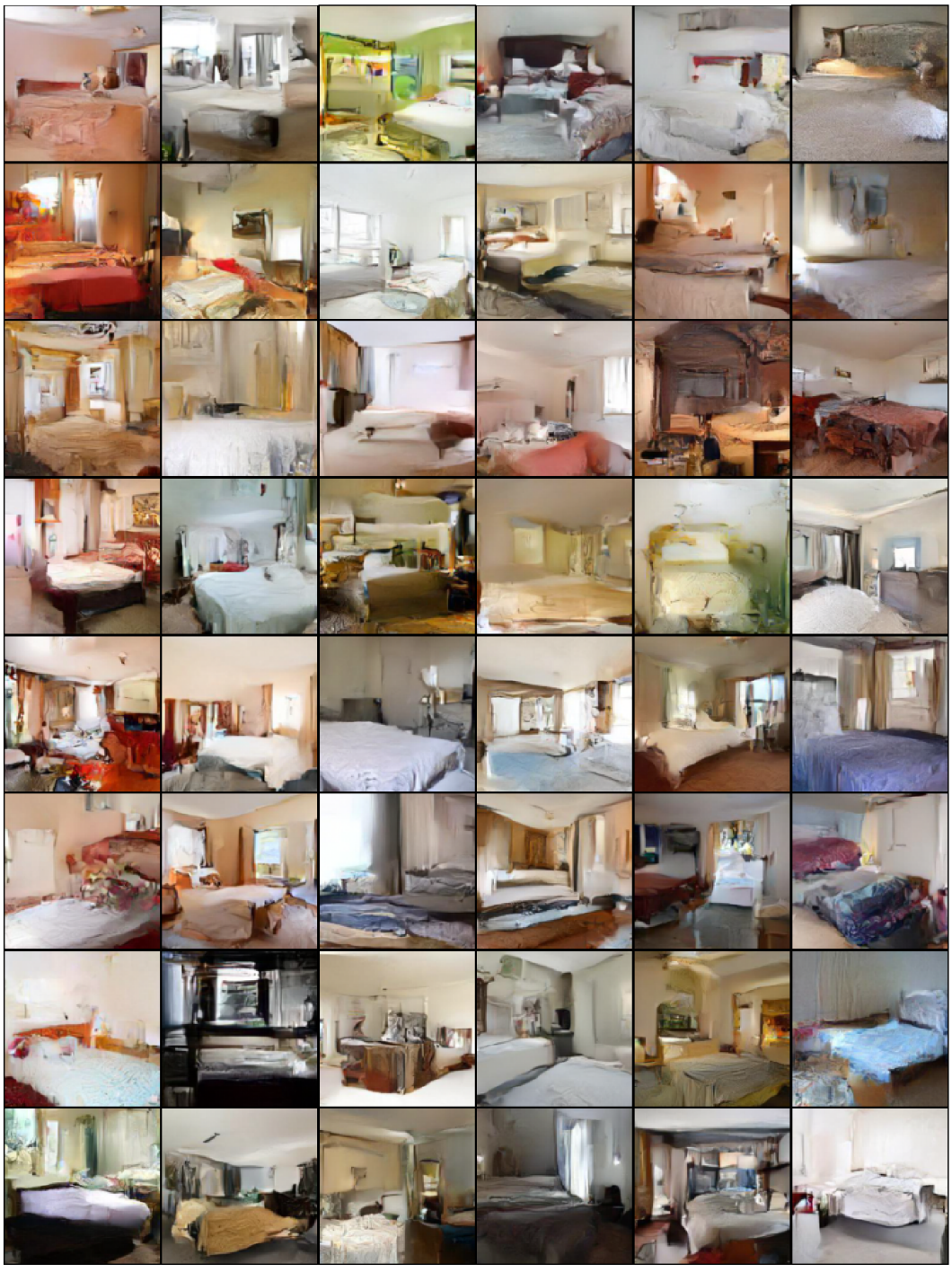

Figure 14: Samples from 8-bit, 128×128 LSUN bedrooms.

F.3 CIFAR-10 & ImageNet

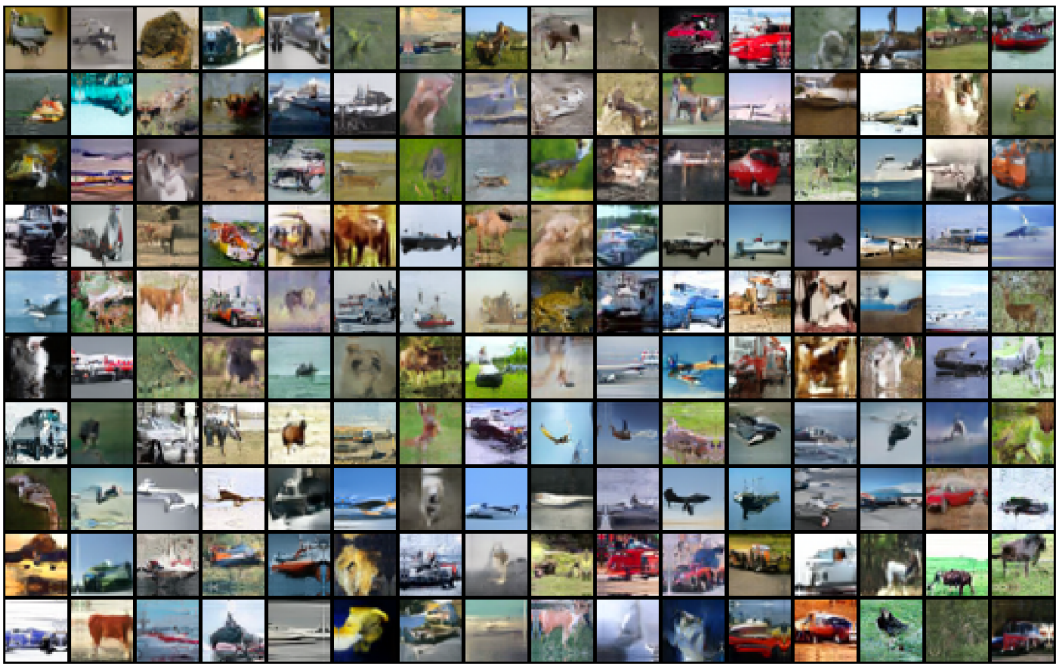

Figure 15: Samples from 8-bit, 32×32 CIFAR-10.

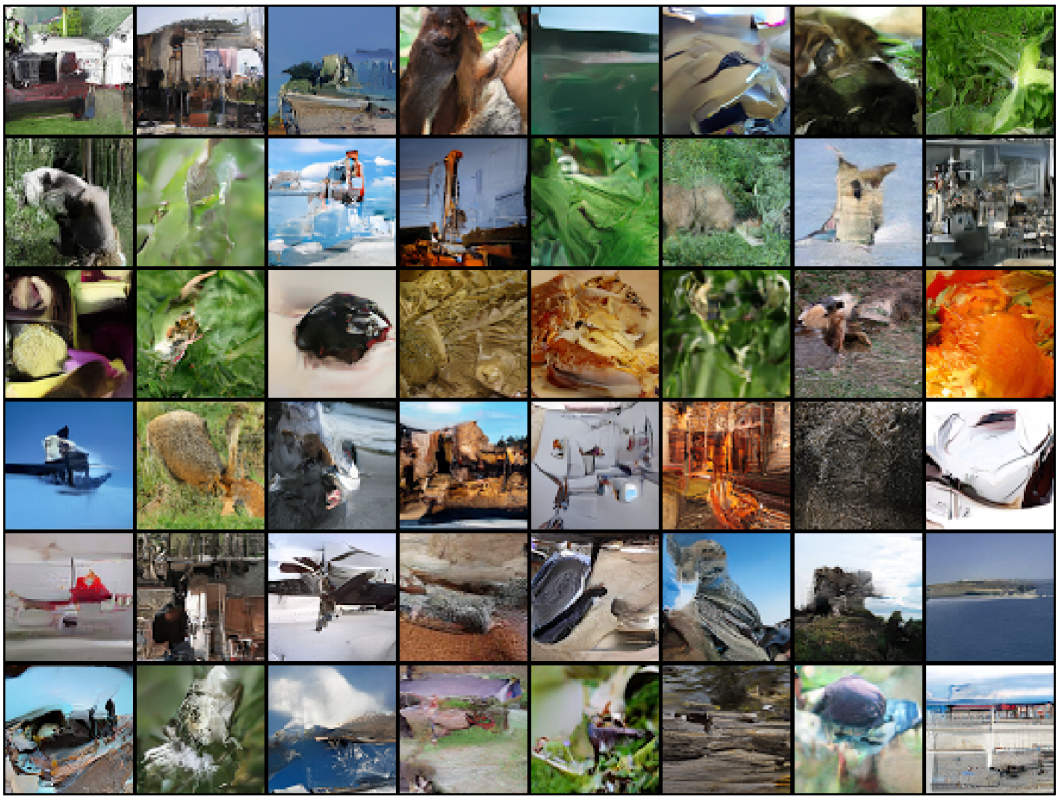

Figure 16: Samples from 8-bit, 64×64 imagenet.